

INTERMEDIATE TURBINE DUCT DESIGN AND OPTIMIZATION

Fredrik Wallin* , Lars-Erik Eriksson* ** , Martin Nilsson**

***Department of Applied Mechanics, Chalmers University of Technology ,**

****Volvo Aero Corporation**

Keywords: optimization, response surface, turbine duct

Abstract

Design improvements of intermediate transition ducts is an area of growing importance. This due to the trend of increasing the radial offset between the low- and high-pressure systems in modern turbo-fan engines. Shape optimization used for turbomachinery applications has become a powerful aero-design tool. Thanks to the rapid development of computer technology, computational fluid dynamics may be used in the optimization process. In the present work the response surface methodology together with design of experiments has been the optimization strategy of choice. An intermediate turbine transition duct containing nine non-lifting struts has been designed and optimized for minimum total pressure loss. The struts are designed from a given duct inlet swirl profile using low-cost streamline calculations. The final design is to be installed in the large-scale low-speed turbine facility at Chalmers for measurements within the EU Sixth Framework Programme project AITEB-2.

1 Nomenclature

Roman

A	Duct flow area
b	Estimated regression coefficients
C_p	Pressure coefficient, $C_p = \frac{p - p^{ref}}{q^{ref}}$
c_1, c_2	Mean line design parameters
d_1, d_2	Height design parameters
h	Duct height

k	Number of design parameters
L	Duct length
m	Duct mean line
n	Number of candidate designs
p	Number of regression coefficients
P	Static pressure
P_i	i^{th} basis function
P_0	Total pressure
q	Dynamic pressure, $q = \frac{1}{2}\rho u^2$
r	Radial co-ordinate
R^2	Coefficient of multiple determination
u	Velocity, $u = \mathbf{u} $, $\mathbf{u} = \{u_x, u_r, u_\theta\}^T$
x	Axial co-ordinate
x_i	i^{th} design parameter
\hat{y}	Estimated response
y^+	Dimensionless wall normal distance

Greek

α	Swirl angle
ζ	Loss coefficient, $\zeta = \frac{\overline{P_{0,in}} - \overline{P_0}}{q_{in}}$
ρ	Density

Subscripts

h	Hub (duct inner-wall)
s	Shroud (duct casing)
in	Inlet
out	Outlet

Superscripts

ref	Reference
$*$	Modified

- Area average
- = Mass flow-weighted average
- ~ Approximate

Abbreviations

BPR	By-Pass Ratio
CFD	Computational Fluid Dynamics
DOE	Design of Experiments
FCCD	Face-Centered Composite Design
HP	High-Pressure
LP	Low-Pressure
RANS	Reynolds-Averaged Navier-Stokes
RSM	Response Surface Methodology

2 Introduction

In multi-spool jet-engines of today the low-pressure (LP) system has a lower rotational speed and a larger radius than the high-pressure (HP) core system. Hence annular S-shaped transition ducts are needed to connect the two systems. The flow in these intermediate ducts is highly complex. It involves strong curvature and many designs have swirling and diffusive flow. There is a risk that endwall separation occurs. Such separations could cause unwanted losses and asymmetric flow distortions. These distortions could have a negative impact on neighboring components. The ducts often have thick structural struts passing through them, since they usually carry loads and support bearings. This makes the ducts large and heavy structures. Improving their design could thus lead to benefits both in weight and performance of the engine. The trend in modern turbo-fan engine design is toward higher by-pass ratios (BPR), which will lead to an increased radial offset between the LP and HP systems and this makes duct design increasingly important. In the present work the design and optimization of a turbine duct has been investigated. Figure 1 shows a typical S-shaped turbine duct.

The use of shape optimization within turbomachinery design is possible today thanks to powerful computer resources for performing computational fluid dynamics (CFD) analysis. Surrogate model-based optimization has in recent

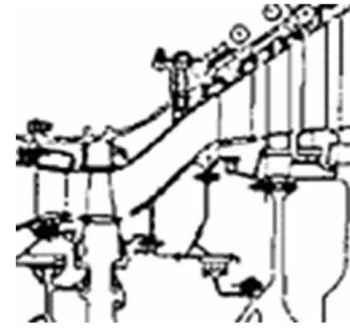


Fig. 1 The turbine transition duct of a high BPR turbo-fan engine.

years become a good alternative to the direct application of gradient-based search algorithms. It is a technique well suited for optimization involving costly CFD analysis. The basic idea of using surrogate models is to construct approximations of the true objective and constraint functions from a set of candidate designs. One such well-known surrogate model approach is the response surface methodology (RSM), which tends to be a robust optimization technique insensitive to numerical noise [1]. RSM is therefore commonly used for global optimization problems. Wallin and Eriksson [2] evaluated the use of RSM for both compressor and turbine transition duct optimization. Papila et al [3] used it for preliminary design optimization of a supersonic turbine and for further investigation of such turbines Papila et al [4] used a method combining radial basis neural networks with RSM. Burman [5] performed compressor blade shape optimization based on RSM. Madsen et al [1] used the method for diffuser shape optimization and Unal et al [6] showed how well RSM works in multi-disciplinary optimization problems.

In this paper the design of an intermediate turbine duct with nine non-lifting struts is described. The struts are designed using low-cost streamline computations. The input to the streamline code is the duct endwalls and an inlet swirl profile. The focus lie on duct endwall shape optimization using CFD together with RSM.

3 Parameterization

A major issue when using RSM is geometry parameterization. As the objective and possible constraints of all candidate designs have been evaluated response surfaces are fitted to the obtained data. In the present work second-order polynomial response surfaces have been used. For this kind of model the number of regression coefficients (p) increases rapidly with the number of design parameters (k), according to the formula $p = (k + 1)(k + 2)/2$. This phenomena is often referred to as the curse of dimensionality. As the number of regression coefficients increases so will the size of the candidate design set. The number of candidate designs (n) used to construct a regression model is $n \geq p$. Since every new design added to the candidate set results in one more CFD analysis, keeping the number of design parameters low is of great importance. In order to keep the design parameters at a minimum, but still obtain maximum flexibility of new designs, an efficient way of modifying the baseline geometry was introduced by Wallin and Eriksson [2]. The idea is to apply perturbations to a baseline duct design. We know that there exists a perturbation such that it optimizes the duct geometry with respect to our defined objective and constraints. Hence an approximation to this perturbation is sought. A linear combination of basis functions is used to construct this approximate perturbation. To ensure that this approximation is the best possible, orthogonal polynomials (P_i) are used as basis functions. All polynomials are defined on the interval $0 \leq x \leq L$, where L is the duct length. The upstream HP turbine and the downstream LP turbine set the duct inlet and outlet radii, flow angles and curvatures. In order not to change these baseline geometrical conditions at inlet or outlet, the boundary conditions (1) are imposed on the orthogonal polynomials.

$$P_i(x) = \frac{dP_i}{dx} = \frac{d^2P_i}{dx^2} = 0 \quad \text{as} \quad \begin{cases} x = 0 \\ x = L \end{cases} \quad (1)$$

The first basis function is defined as the lowest order non-zero polynomial satisfying these

boundary conditions. The second basis function is the lowest order non-zero polynomial that satisfies the boundary conditions (1) and is orthogonal to the first basis function according to the scalar product (2).

$$\int_0^L P_i(x) P_j(x) dx \quad \begin{cases} = 0 & \text{as } i \neq j \\ \neq 0 & \text{as } i = j \end{cases} \quad (2)$$

Adopting this procedure results in the two basis functions shown in figure 2. An infinite number of orthogonal polynomials can be defined, but in the present work only the first two have been used. These basis functions take the form of equation (3).

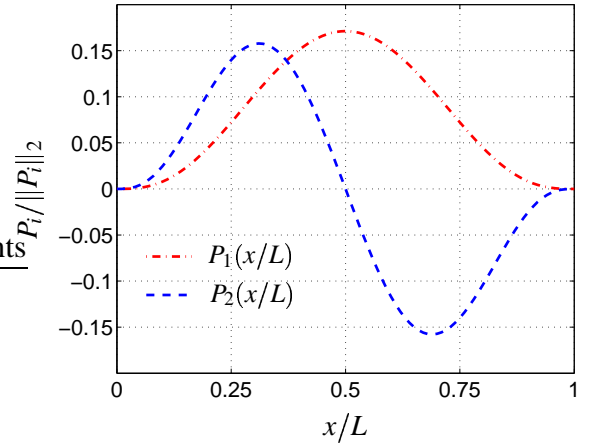


Fig. 2 The two orthogonal polynomials used as basis functions.

$$\begin{aligned} P_1(x) &= x^3 (L - x)^3 \\ P_2(x) &= x^3 (L - x)^3 \left(\frac{L}{2} - x\right) \end{aligned} \quad (3)$$

The reference geometry is modified by adding perturbations to two functions approximately corresponding to the duct mean line and height distribution respectively. These perturbations consist of linear combinations of the orthogonal polynomials defined. Having the mean line and height represent the duct geometry instead of the hub and shroud curves result in two functions with greater influence on and stronger coupling to the duct flow field. The approximate mean line (\tilde{m}) and height (\tilde{h}) are defined by equation (4).

$$\begin{aligned}\tilde{m}(x) &= \frac{1}{2}r_s(x) + \frac{1}{2}r_h(x) \\ \tilde{h}(x) &= r_s(x) - r_h(x)\end{aligned}\quad (4)$$

Here r_h and r_s are the hub and shroud radii respectively. Commonly a duct geometry is described by defining its mean line and area distribution. In the present work the height distribution was chosen over the area distribution to avoid the non-linearity associated with area calculations. To further simplify the parameterization, both functions describing the duct geometry (\tilde{m} and \tilde{h}) and also the basis functions (P_i) have been parameterized along the axial co-ordinate x . A parameterization along a streamwise co-ordinate was considered, but would introduce problems with maintaining the reference design inlet and outlet angles and curvature. Modifications to the reference geometry are done by assigning certain values to the design parameters (c_1, c_2, d_1 and d_2). These design parameters are then used as coefficients multiplying the basis functions. Equation (5) shows how the modified mean line (\tilde{m}^*) and height distribution (\tilde{h}^*) are calculated.

$$\begin{aligned}\tilde{m}^*(x) &= \tilde{m}^{ref}(x) + c_1P_1(x) + c_2P_2(x) \\ \tilde{h}^*(x) &= \tilde{h}^{ref}(x) + d_1P_1(x) + d_2P_2(x)\end{aligned}\quad (5)$$

The new duct design obtained, i. e. the modified hub (r_h^*) and shroud (r_s^*), is now described by equation (6).

$$\begin{aligned}r_h^*(x) &= \tilde{m}^*(x) - \frac{1}{2}\tilde{h}^*(x) \\ r_s^*(x) &= \tilde{m}^*(x) + \frac{1}{2}\tilde{h}^*(x)\end{aligned}\quad (6)$$

4 Numerics

An in-house compressible flow solver [7], has been used for all CFD analyzes. The code is based on a cell-centered finite-volume approach, adapted to a structured multi-block grid, to solve the governing compressible RANS equations. Third order upwinding is used for the convective

flux and the upwinding biasing is based on local characteristic variables and speeds. A three-stage Runge-Kutta method is used for the time-marching. Turbulence is modeled using a realizable k- ϵ closure with standard wall-functions. The cell-centers adjacent to the endwalls were located at an average of $\overline{y^+} \approx 45$. For the strut-adjacent cell-centers $\overline{y^+} \approx 30$ was obtained.

A 40°-sector of the duct with rotationally periodic interfaces on the sides has been used for all CFD analyzes. The computational domain is presented in figure 3. Axi-symmetric inlet profiles prescribing values on total pressure and enthalpy and on two angles defining the swirl and radial velocity components have been used. Typical turbulence intensities and length scales were also assumed at the inlet boundary. At the outlet boundary, which has been extended 0.2L downstream, the static pressure is prescribed.

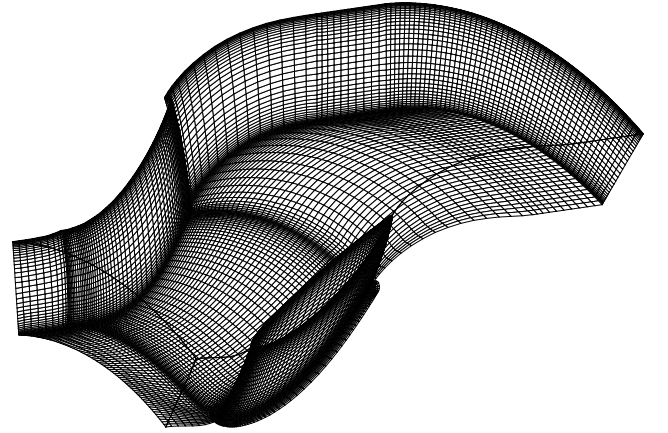


Fig. 3 The computational domain and examples of the surface mesh of the baseline duct.

5 Optimization Procedure

The optimization procedure when using RSM consists of three steps. First a design space is defined and spanned by user-defined design parameters. A low number of individual geometry samples (candidate designs) within the design space are chosen, according to the theory known as design of experiments (DOE). These designs constitute the candidate data set from which a re-

gression model can be constructed. In the present work a face-centered composite design (FCCD) has been adopted producing $n = 2^k + 2k + 1$ candidate designs. Figure 4 shows the normalized design space spanned by the four design parameters used (c_1, c_2, d_1, d_2). The locations of each of the $n = 25$ candidate designs are illustrated by dots.

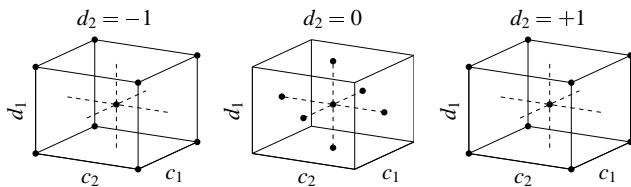


Fig. 4 The 4-dimensional design space.

Secondly the objective function is evaluated for each candidate design using CFD and a least-squares approximation is used to construct a response surface approximation of the objective function. Additional response surfaces for possible constraints may be constructed in the same manner. In the present work a second-order polynomial regression model has been used. For this type of model the estimated response has the form of equation (7).

$$\hat{y} = b_0 + \sum_{i=1}^k b_i x_i + \sum_{i=1}^k b_{ii} x_i^2 + \sum_{i < j=2}^k b_{ij} x_i x_j \quad (7)$$

Here \hat{y} is the approximation of the true response. The b 's are thus the estimators of the regression coefficients and x_i is the i^{th} design parameter. As a measure of the quality of the response surface fit the coefficient of multiple determination R^2 may be used. However the adjusted coefficient, R^{2*} , is a better statistic [5]. It is obtained by scaling the terms involved in finding R^2 by their associated degrees of freedom. A value of $R^{2*} = 1.0$ would correspond to a perfect response surface fit, i. e. the surrogate model predicts the exact same response as the CFD analysis for each candidate design.

The third and final step is to find the optimum of the approximate objective function constructed. This is now a simple operation, since

our response surface is an analytical expression. Therefore a low-cost gradient-based search algorithm can be used to find the optimum. In this work a sequential quadratic programming method is adopted to solve the optimization problem [8]. For a detailed description of DOE and RSM, the book by Myers and Montgomery [9] should be consulted.

6 3D Turbine Duct Design

The non-dimensional numbers describing the duct geometry were given by the large-scale low-speed turbine facility at Chalmers [10]. Table 1 contains these numbers. Here $\Delta m = m_{out} - m_{in}$, which is the change in mean line radius from the duct inlet to outlet. To fit the outlet of the installed turbine, the hub and shroud inlet radii were fixed.

Table 1 The non-dimensional numbers of the turbine duct.

Area ratio	A_{out}/A_{in}	1.60
Non-dimensional length	L/h_{in}	4.55
Aspect ratio	$L/\Delta m$	2.47

Turbine ducts are commonly classified using the diagram by Sovran and Klomp [11], developed for determining optimum geometries for rectilinear diffusers with annular cross-sections. Adopting this classification would reveal the investigated duct to be fairly aggressive as seen in figure 5. An important note is that this classification does not include the duct aspect ratio nor effects due to curvature or swirl. Neither does it take the important effects of any blading present in the duct into account.

A baseline duct design was constructed by using a fifth order polynomial as mean line and another fifth order polynomial as area distribution. This area distribution was then slightly modified to account for some of the blockage caused by the struts. Doing so results in a more reasonable baseline design. In figure 6 the baseline area distribution used is plotted. Combining this area

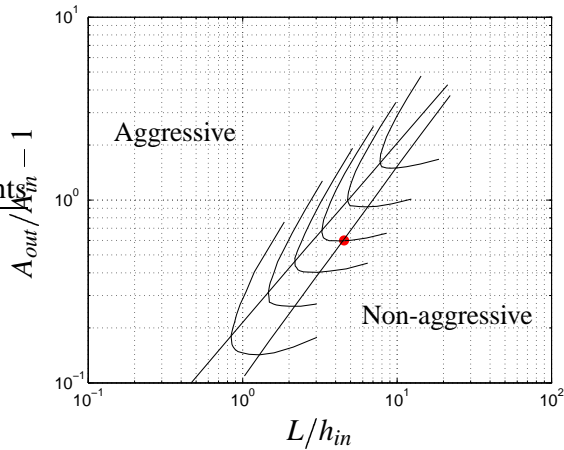


Fig. 5 Classification of baseline duct.

distribution with the fifth order polynomial mean line defined results in the baseline duct geometry presented in figure 7.

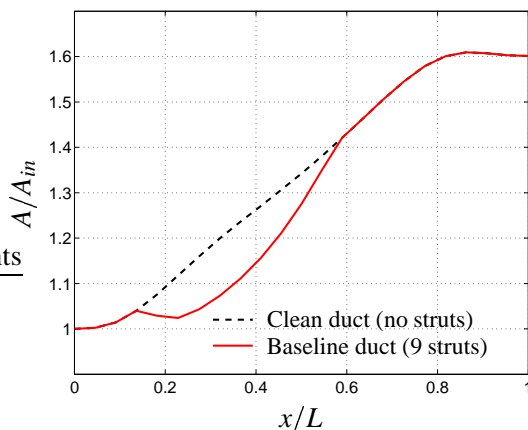


Fig. 6 The baseline duct area distribution.

6.1 Strut Design

The struts are designed through a low-cost and rather simple process. A number of camber lines at different spans are defined, as will be described later. A predefined thickness distribution is applied to each of these camber lines. The thickness distribution used in the present study is that of a modified NACA four digit-series airfoil [12]. The modifications to the original profile include a thicker trailing edge and a modified leading edge. The location of maximum thickness is also not fixed, but can instead be placed arbitrarily. The

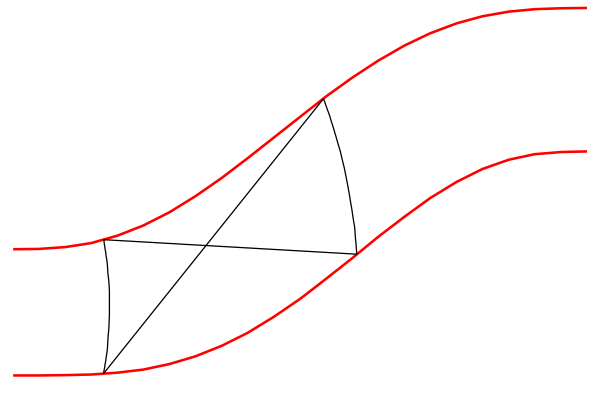


Fig. 7 The baseline duct design.

design philosophy is to have a non-lifting strut, i.e. the airfoil constructed should not take any net aerodynamic load at the design point of the upstream turbine. Thus the camber lines should follow the swirl distribution of the duct flow in a clean duct (without struts). From the turbine outlet conditions and a given duct geometry, i. e. the duct endwalls, the gas channel is divided into streamtubes. The curvature of each streamtube is calculated through conservation of mass and angular momentum. The area distribution is calculated accounting for strut blockage. Doing so is possible since the strut thickness distribution is predefined. Furthermore all streamtubes are assumed to have an equal amount of diffusion. The geometrical parameters of the strut were chosen according to common industry practice. The strut is stacked at maximum thickness to allow for servicing tubes through it and to permit it to carry radial load. In addition, the leading and trailing edges have been designed to be similar to those of existing engine designs (see figure 7), as has the solidity. The struts are all identical and equally distributed circumferentially. The strut count was chosen to allow for periodicity when performing calculations of the duct including the stator and rotor blades of the upstream turbine. The turbine stage consists of 36 stator blades and 72 rotor blades. For each new candidate design produced during the optimization process a strut design fitting the endwalls of that particular duct is constructed. This is a straight-forward operation, since the strut geometry is a function of the

duct endwalls and the inlet swirl profile only.

Once the baseline endwalls were defined a baseline strut was designed. The duct inlet swirl profile presented in figure 8 was given by the turbine outflow. Here the swirl angle α is defined by $\sin \alpha = u_\theta/u$. The significant change in swirl angle toward the shroud is due to the 1.5% tip-leakage of the turbine rotor blades.

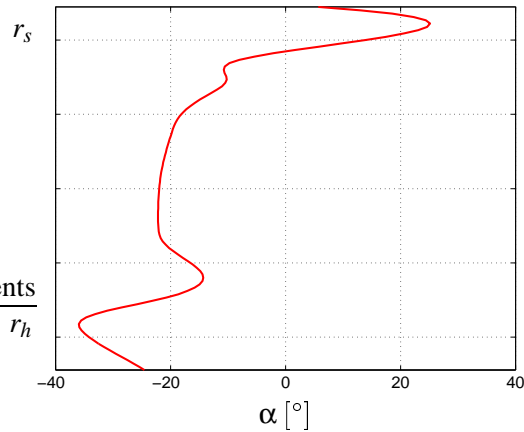


Fig. 8 The duct inlet swirl profile.

The mean value of the inlet swirl angle, $\bar{\alpha} \approx 17^\circ$, was then used as input to the non-lifting strut design calculations. This will result in a locally loaded strut. However the net lifting force on the strut should be kept close to zero. In figure 9 the pressure distribution on the strut design of the baseline duct is presented at three different spans. There are large variations in the strut load, as expected since it was designed for a constant inlet swirl angle. Noticeable is the pressure plateau at 90% span, which indicates a region of separated flow on one side of the strut (this will be shown in more detail later).

7 Results

In the present work the main objective has been to minimize the overall duct pressure loss coefficient defined by equation (8)

$$\zeta_{out} = \frac{\overline{P_{0,in}} - \overline{P_{0,out}}}{\overline{q_{in}}} \quad (8)$$

The unconstrained optimization problem to solve is described by equation (9).

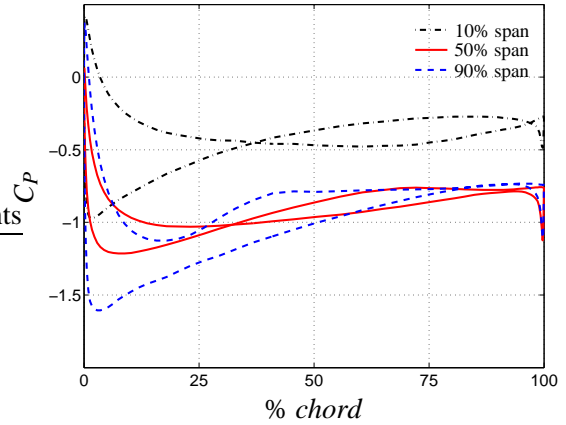


Fig. 9 The pressure distribution of the strut in the baseline duct.

$$\text{minimize } \zeta_{out}(c_1, c_2, d_1, d_2) \quad (9)$$

A comparison of the overall duct losses shows that a loss reduction of 25% was obtained by optimization and re-design. The optimization was performed in two steps. First a large design space was setup and an intermediate optimum design found (RS_1). Then a second refined design space was constructed around the intermediate optimum and a final optimum design obtained (RS_2). The quality of fit statistics (R^{2*}) of both response surfaces is quite good and the accuracy is also confirmed by comparing the predicted losses from the surrogate models (RS_1 and RS_2) to the losses obtained from additional CFD analyzes of the optimum designs (CFD_1 and CFD_2). Table 2 summarizes the optimization results.

Table 2 The optimization results.

	ζ_{out}	Change	R^{2*}
Baseline	0.199	–	–
RS_1	0.157	–21%	0.99
CFD_1	0.154	–23%	–
RS_2	0.150	–25%	0.95
CFD_2	0.149	–25%	–

In figure 10 the optimum design obtained is compared to the baseline duct. The new design seems to primarily compensate for the strut

blockage and opens up in the strut region. Figure 11 shows a comparison between the baseline and optimum area distributions. An early rapid diffusion seems to be a favorable mechanism for reducing losses. Interestingly a significant contraction in the region of the strut trailing edge is observed. This will result in a local flow acceleration, which works to restrain boundary layer separation in the most critical area of the duct.

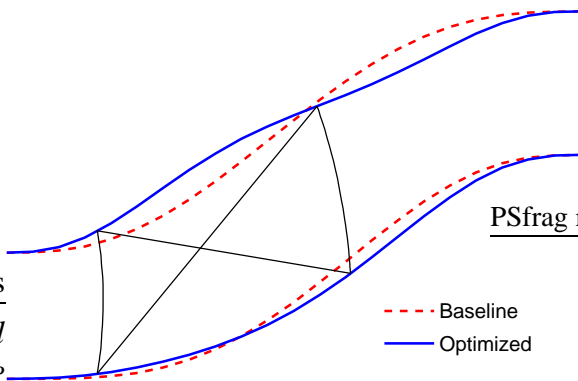


Fig. 10 The baseline vs. optimized duct design.

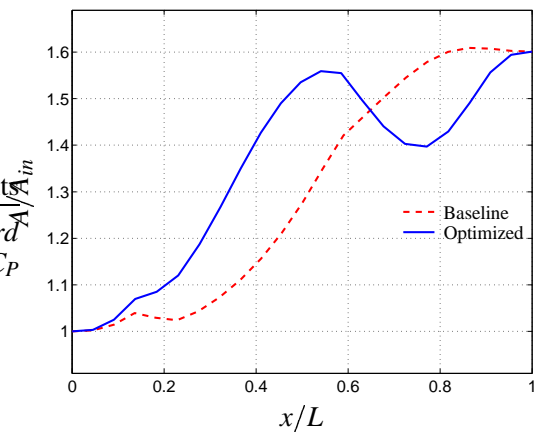


Fig. 11 The baseline vs. the optimized duct area distribution.

A re-design of the duct endwalls will also cause the strut pressure distribution to change. Figure 12 shows the static pressure coefficient at three different spans of the strut in the optimized duct. When compared to the baseline strut pressure distribution (figure 9) it seems the strut of the re-designed duct has a more non-lifting be-

havior, as desired. The strut is not perfectly non-lifting, but takes a small net load. This load approximately corresponds to a change in swirl angle $\Delta\alpha \approx 2.5^\circ$ from the leading to trailing edge of the strut. As concluded earlier the optimization acts to accelerate the flow in the region of the strut trailing edge. This will result in a weaker adverse pressure gradient, which leads to a less loaded boundary layer.

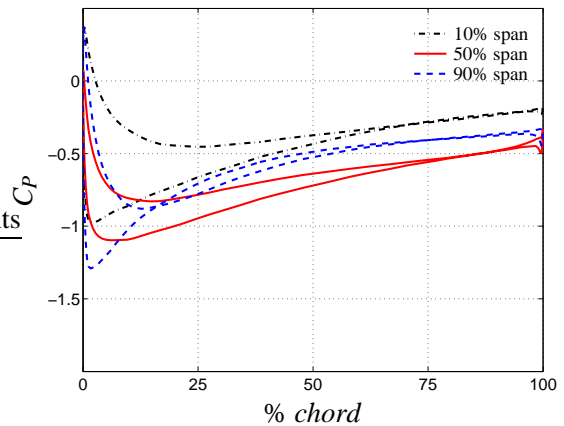


Fig. 12 The pressure distribution of the strut in the optimized duct.

Figure 13 attempts to visualize the loss development throughout the duct. The loss coefficient has been evaluated at axi-symmetric planes perpendicular to the duct mean line. It can be seen that the loss of the baseline duct starts to diverge rapidly from that of the optimized duct close to the point of the strut maximum thickness. This is due to the major separation occurring in the strut/shroud corner of the baseline duct.

Iso-surfaces of negative axial velocity in the vicinity of the strut in the baseline duct are shown in figure 14. As has been discussed, a less loaded strut boundary layer can be obtained by re-designing the duct endwalls. Minimizing the total pressure loss also works to reduce possible boundary layer separation. Thus using the total pressure loss coefficient as objective seems to be a suitable approach for suppressing regions of separation. Figure 15 shows iso-surfaces of negative axial velocity in the optimized duct. When compared to figure 14 it is clear that the optimization has a significant impact on the regions

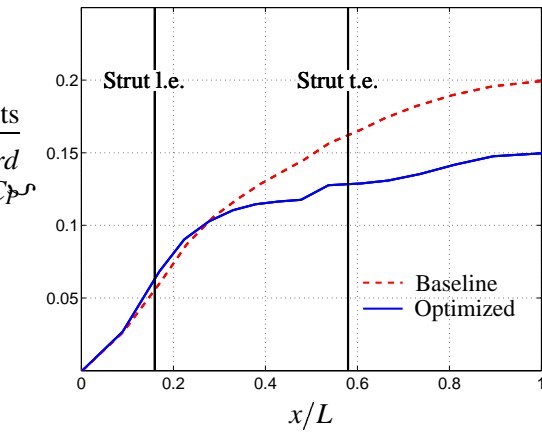


Fig. 13 Development of losses throughout the ducts.

of negative axial velocity. Small corner separations are difficult to suppress, but might disappear if fillets were to be introduced between the strut and endwalls. However this duct is a low-speed design to be installed in a testing facility and small regions of separation are acceptable.

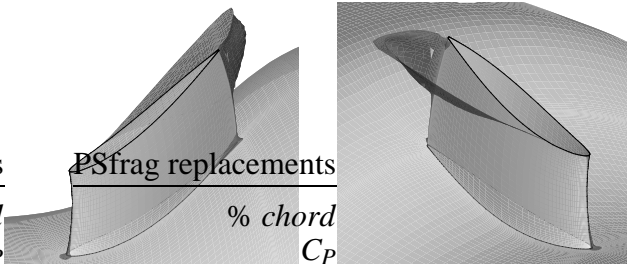


Fig. 14 Iso-surfaces of negative axial velocity in the strut region of the baseline duct.

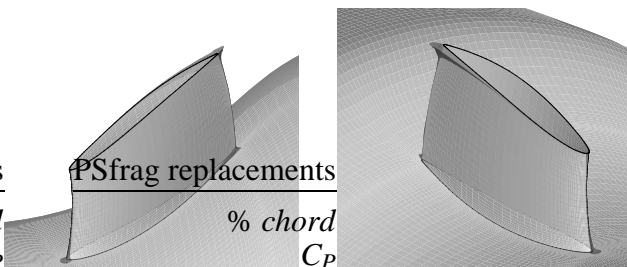


Fig. 15 Iso-surfaces of negative axial velocity in the strut region of the optimized duct.

Figure 16 shows contours of the local loss

coefficient at the outlets of the baseline and optimized duct respectively. It can be concluded that the optimization influences the wake behavior in a beneficial way. The baseline duct outlet wake is thicker and deeper than the one of the optimized duct. Due to the massive separation, seen in figure 14, a large high-loss region is observed at the baseline duct outlet.

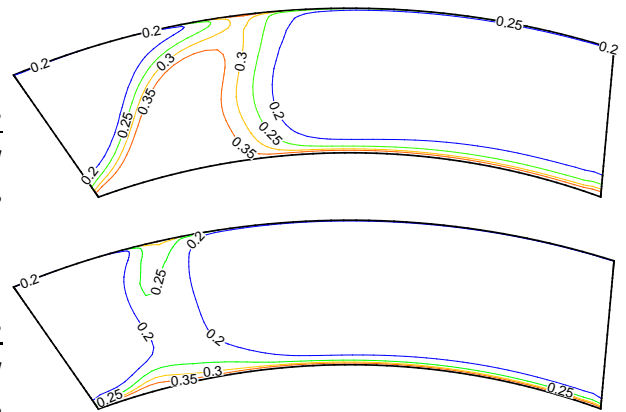


Fig. 16 Outlet contours of the baseline (top) and optimized (bottom) loss coefficient.

8 Conclusions

For transition ducts the use of RSM together with DOE seems to be a suitable approach for exploring the design space and deciding on regions of feasible designs. Since orthogonal polynomials are used to modify the baseline duct shape, a wide variety of designs are possible to produce by introducing only a low number of design parameters. The idea of applying perturbations to a reference design is particularly attractive for redesign purposes. Via optimization a loss reduction of 25 % was obtained for the turbine duct investigated. However the magnitude of improvement in this particular case is highly dependent on the poor baseline design. Still the results indicate that a significant loss reduction is possible to obtain if shape optimization is included in the duct design process.

The optimized design obtained indicates some possible mechanisms for reducing duct

losses and suppressing boundary layer separations. A rapid diffusion in the beginning of the duct results in a local area decrease in the later part of the duct. Thereby an acceleration of the flow is obtained in a region where separation is likely to occur. The optimization causes the duct to compensate for blockage by increasing its area in the strut region, which results in a weaker adverse pressure gradient along the shroud. Also the significant changes of the shroud slope in this region affect the local flow characteristics in the separated region of the baseline duct. A stronger streamwise curvature toward the duct outlet is observed for the optimized design. This shift of curvature seems to be beneficial for reducing losses within the duct, but might affect the inflow to downstream components in a negative way. Such effects have not been investigated in the present work, since the final duct design is intended for a turbine testing facility without critical downstream components. Incoming wakes and radial distortion effects are also neglected in the analyzes performed here. No constraints on the geometry nor on any flow parameters have been considered either.

9 Acknowledgment

This work was conducted within the EU FP6 Project AITEB-2 (Aerothermal Investigations on Turbine Endwalls and Blades), contract number: AST4-CT-2005-516113.

References

- [1] J. I. Madsen, W. Shyy, and R. T. Haftka. Response Surface Techniques for Diffuser Shape Optimization. *AIAA Journal*, 38:1512–1518, 2000.
- [2] F. Wallin and L.-E. Eriksson. Response Surface-based Transition Duct Shape Optimization. Barcelona, Spain, 2006. ASME Turbo Expo 2006, GT-2006-90978.
- [3] N. Papila, W. Shyy, L. Griffin, F. Huber, and K. Tran. Preliminary Design Optimization for a Supersonic Turbine for Rocket Propulsion. Huntsville, Alabama, 2000. 36th AIAA/ASME/SAE/ASEE Joint Propulsion Conference and Exhibit, AIAA-2000-3242.
- [4] N. Papila, W. Shyy, L. Griffin, and D. J. Dorney. Shape Optimization of Supersonic Turbines Using Global Approximation Methods. *Journal of Propulsion and Power*, 18:509–518, 2002.
- [5] J. Burman. *Geometry Parameterisation and Response Surface-Based Shape Optimisation of Aero-Engine Compressors*. PhD thesis, Department of Applied Physics and Mechanical Engineering, Luleå University of Technology, Luleå, 2003.
- [6] R. Unal, R. A. Lepsch, and M. L. McMillin. Response Surface Model Building and Multidisciplinary Optimization Using D-optimal Designs. St. Louis, Missouri, 1998. 7th AIAA/USAF/NASA/ISSMO Symposium on Multidisciplinary Analysis and Optimization, AIAA-1998-4759.
- [7] L.-E. Eriksson. Development and Validation of Highly Modular Flow Solver Versions in G2DFLOW and G3DFLOW. Internal report 9970-1162, Volvo Aero Corporation, Sweden, 1995.
- [8] P. T. Boggs and J. W. Tolle. Sequential Quadratic Programming. In *Acta Numerica*, pages 1–51. 1995.
- [9] R. H. Myers and D. C. Montgomery. *Response Surface Methodology*. John Wiley & Sons, Inc., 2nd edition, 2002. ISBN 0-471-41255-4.
- [10] C. Arroyo, L.-U. Axelsson, U. Håll, T. G. Johansson, J. Larsson, and F. Haselbach. Large Scale Low Speed Facility for Investigating Intermediate Turbine Duct Flows. Reno, Nevada, 2006. 44th AIAA Aerospace Sciences Meeting and Exhibit, AIAA-2006-1312.
- [11] G. Sovran and E. D. Klomp. *Experimentally Determined Optimum Geometries for Rectilinear Diffusers with Rectangular, Conical or Annular Cross-section*. Fluid Mechanics of Internal Flow, Elsevier Publishing Co., G. Sovran edition, 1967.
- [12] I. H. Abbot and A. E. von Doenhoff. *Theory of Wing Sections*. Dover, 1949; reprinted 1958. ISBN 0-486-60586-8.